Impact of flax fibre micro-structural features on composite damage observed through micro-CT characterisation

Elouan Guillou, Andrew King, Jonathan Perrin, Henry Proudhon, Timm Weitkamp, Darshil Shah, Alexandre Beigbeder, Pierre Ouagne, Alain Bourmaud

▶ **To cite this version:**

Elouan Guillou, Andrew King, Jonathan Perrin, Henry Proudhon, Timm Weitkamp, et al.. Impact of flax fibre micro-structural features on composite damage observed through micro-CT characterisation. Composites Part A: Applied Science and Manufacturing, 2024, 181, pp.108118. 10.1016/j.compositesa.2024.108118 . hal-04803642

HAL Id: hal-04803642
https://hal.science/hal-04803642v1

Submitted on 25 Nov 2024

HAL is a multi-disciplinary open access archive for the deposit and dissemination of scientific research documents, whether they are published or not. The documents may come from teaching and research institutions in France or abroad, or from public or private research centers.

L'archive ouverte pluridisciplinaire **HAL**, est destinée au dépôt et à la diffusion de documents scientifiques de niveau recherche, publiés ou non, émanant des établissements d'enseignement et de recherche français ou étrangers, des laboratoires publics ou privés.

Impact of flax fibre micro-structural features on composite damage observed through micro-CT characterisation

*Elouan Guillou[a,b], Andrew King[c], Jonathan Perrin[c], Henry Proudhon[d], Timm Weitkamp[c], Darshil U. Shah[e], Alexandre Beigbeder[a], Pierre Ouagne[f], Alain Bourmaud[b]

[a] IPC Laval, Rue Léonard De Vinci, 53810 Changé, France

[b] Univ. Bretagne Sud, UMR CNRS 6027, IRDL, F-56100 Lorient, France

[c] Synchrotron SOLEIL, F-91190 Saint-Aubin, France

[d] PSL University, MAT -- Centre des matériaux, CNRS UMR 7633, BP 87,F- 91003, Evry, France

[e] Centre for Natural Material Innovation, Department of Architecture, University of Cambridge, Cambridge CB2 1PX, UK

[f] Laboratoire Génie de Production, LGP, Université de Toulouse, INP-ENIT, 65000 Tarbes, France

*Corresponding author: elouan.guillou@ct-ipc.com

Abstract

To exploit the potential of flax fibres in reinforcing polymers, the performance of flax fibres must first be understood and then optimized. In this context, this paper aims to provide a visual and comprehensive description of the impact flax fibre micro-structural features, such as kink bands, porosity and cortical residues, have on damage evolution during tensile loading of Polylactic acid (PLA) matrix composites reinforced by flax fibres. *In-situ* synchrotron radiation computed tomography (SRCT) has been used for 3D visualisation of microstructural evolution at stress levels between 10% and 90% of the ultimate failure stress. First, the main defects of the overall microstructure are described, including a quantitative analysis of porosities. Then, novel visual insights, highlighting the main role of kink-bands in fibre failure and subsequent composite breakage, are described. Interestingly, it appears that for the flax/PLA composite studied, kink-band inter-distances are consistently smaller than critical fibre lengths,

explaining the likelihood of rupture in kink-band regions. These findings demonstrate that fibre extraction and subsequent textile reinforcement manufacturing are critical steps and should be optimised to increase the performances of natural fibre composites.

Keywords: A-Microtomography; B-Microstructure; B-Defects; D- *In-situ* synchrotron radiation computed tomography (SRCT)

1. Introduction

The potential for reinforcement of polymers by flax fibres has been demonstrated over the last 80 years [1] and their use in the composites industry has developed considerably over the past 20 years. Motivated by climate change and the need to drastically reduce the consumption of fossil-based resources, flax fibres have gained interest in many industrial sectors [2,3]. The high specific mechanical properties of elementary flax fibres indicate that they can be a competitive alternative to traditional synthetic reinforcements such as glass fibres. However, the strength of flax fibre composites often remains below the expected mechanical properties for flax fibre reinforcements. This raises the question of early failure of the material induced by microstructural heterogeneity or defects. Inevitably, composite manufacturing may induce defects, such as fibre misalignment or void formation, but composite failure mechanisms also relate to the specific micro-structural features of flax fibre reinforcements. In particular, the reinforcement potential can be affected by the presence of structural fibre defects, called kink-bands, which are sensitive areas. Kink-bands are structural irregularities of the fibre cell wall, highlighted by intense local mis-orientation of cellulose macro-fibrils (locally up to 30-40°) [4] and rings of pores forming at cellulose layer interfaces in the gelatinous bulk [5]. Even if there is some controversy in the literature, it has been shown that the presence of kink-bands negatively affects the tensile strength of the fibres [6, 7]. At the composite scale, these dislocation zones are known to give rise to matrix stress concentrations, leading to fibre failure and crack propagation within the surrounding matrix [8]. Recent works have highlighted, through observations *in-planta* and on extracted fibres, that kink-band development is mainly induced by the fibre extraction process (retting, scutching and hackling) [9, 10] and not during the growing or retting of the plants. However these extraction steps

52 are crucial for fibre individualisation, reducing the number of aggregate fibre bundles in the final
53 composite and ultimately contributes to an increase in tensile strength [11]. While the micro-structural
54 features of flax fibres are being increasingly documented, their impact on composite damage needs
55 more evidence and interpretation.

56 In order to optimise plant fibre reinforcements for load-bearing applications, it is necessary to
57 gain further insight into failure mechanisms of flax fibre composites [12]. Many post-failure analysis
58 techniques, such as optical and SEM observation, can be commonly used to investigate failure areas but
59 do not allow the observation of damage evolution during composite loading. Other methods such as
60 Digital image correlation (DIC) or acoustic-emission are suitable for detection of a wide range of cracks
61 and structural failures during composite loading but still not provide any internal visual insight. X-ray
62 micro-computed tomography (micro-CT) is an adequate tool for the investigation and characterisation
63 of the internal 3D structure of composites and to visualise defects [13,14]. Combining micro-CT with
64 tensile testing is a powerful technique to understand the impact of defects on damage evolution within
65 composites [15].

66 In the present work, the three-dimensional microstructural damage evolution of unidirectional
67 (UD) flax fibre reinforced Polylactic Acid (PLA) composites is studied through in-situ tomography during
68 loading until failure. The overall microstructure and principal defects in the composite are first
69 presented. This description has been enhanced by micro-CT observations obtained at the bundle scale
70 on isolated dry flax bundles. Then, we analyse the specific role each type of defect plays in composite
71 damage mechanisms, followed by a discussion on optimising flax fibre reinforcements.

72

73 **2. Materials and methods**

74 **2.1. Materials**

75 Lightweight unidirectional flax preforms (Flaxtape®, 100 g/sm), provided by Ecotechnilin
76 (Yvetot, France), were used to make composites. PLA was chosen as a matrix due to its superior
77 adhesion properties with flax at microscopic scale, compared to non-grafted polyolfines and other

biodegradables polymers [16]. In addition, unlike non-biodegradable polymers, PLA offers alternative end-of life scenarios such as industrial composting [17]. The PLA granulates were provided by NatureWorks (PLA3001D). They have a density of 1.24 g/cm³ and a melt flow index (MFI) of 22 g/10 min (210 °C/2.16kg).

2.2. Composite manufacturing

Unidirectional composites were manufactured following the film stacking process, based on the parameters used by Pantaloni et al. [18]. First, PLA granulates were dried for 12h at 55°C under vacuum. Then, PLA films were manufactured by cast film extrusion using a mono-screw extruder (Labstation Plasticorder Brabender) and a Univex Brabender (Bradender, Duisburg, Germany) calendaring machine. The PLA films obtained have a thickness around 100 µm. PLA films and flax preforms were then cut to mould size using a rotary cutter. The lay-up was comprised of 16 plies of flax and several intermediate plies of PLA films for a unidirectional composite $[0]_{16}$. A fibre weight fraction of (48 ± 2) % was achieved and checked by the density method.

Once manufactured, laminates were cut using a laser machine Arketype (Amiens, France), according to the shape shown in Figure 1.D. Small tensile specimens were specifically designed for this study. They were notched to ensure that damage developed in a well-defined area (Fig.1.D). 0.5 mm thick aluminium tabs were glued with an epoxy resin at each end of the specimens to facilitate the mounting of the specimens in the loading fixture.

2.3. Tensile testing

Tensile tests were performed using an electro-mechanical tension machine (see Fig.2) designed for in-situ micro-CT experiments. The lower cross head speed was controlled by a stepper motor (Phytron ZSS 52.200.1,2 GPL 52/3). The force applied to the specimen was continuously measured by a load cell (FUTEK SERIE LCM 300 ± 1000 lbs). In order to monitor tensile tests from the beamline acquisition system, the machine was plugged directly into the synchrotron electronic system. The load frame consist of a 3mm thick PMMA tube with a diameter of 18 mm (see Fig. 2(a)), presenting constant absorption to X-rays during the rotation.

Initial specimens were tested at 0.02mm/min between each scan, occurring every 45 seconds. For each specimen, the resulting 12 tomographic scans were carefully inspected to identify the stress levels at which first microstructure damage occurs. Among tested samples, no damage was observed below 138 MPa. Above 150 MPa some scans resulted in blurry images, so no damage growth was observable until the composite breaks. Therefore, only 4 scans (see Fig.2c) were selected at 12 MPa (initial state), 138MPa (before any visible damage), 150 MPa (some visible damage) and after failure. These are described in section 3.

2.4. Synchrotron Radiation Computed Tomography (SRCT)

X-ray microtomography scans were recorded on two beamlines at the SOLEIL synchrotron. In both setups, the detector was a standard indirect design with a $Lu_3Al_5O_{12}$:Ce scintillator (Crytur, Turnov, Czech Republic) and a CMOS- based camera (Hamamatsu ORCA Flash 4.0 V2) with 2048 × 2048 pixels of physical size 6.5 µm, coupled via microscope optics to obtain an effective pixel size in the sub-micrometer range. The scans were made on-the-fly, i.e., the sample kept rotating during image acquisition. Volumes were reconstructed using the open-source software PyHST2 (ESRF, Grenoble, France) (Mirone et al., 2014).

At the composite scale, SRCT scans were recorded on the PSICHE beamline. The setup used a pink beam with an average detected photon energy around 28.5 keV. Energies above 41 keV were filtered by the X-ray mirror set at 2 mrad, after the fixed absorbers (CVD diamond and silicon carbide). Further filtering results in a beam spectrum defined by a tin absorption edge at 29.2 keV, a full width at half maximum bandwidth of around 2.8 keV and a peak intensity at 29 keV. A flux of about 10^{13} photons/s/mm^2 was estimated at sample position. The specimen was vertically aligned and centred on the rotation axis of the grips. As the specimen fit in the acquisition window, a single scan was performed for each loading step. Attenuated X-rays through the tube and the sample formed a radiograph on a 50 micron thick scintillator, and were collected by the detector via 10x magnifying optics. A tomography scan corresponded to a set of 1000 radiographs, recorded over a 180° rotation. Exposure time was set to 20 ms, resulting in scan duration of ~33 s for the acquisition of a complete set of radiographs. The camera was positioned at 40mm from the specimen to obtain a good combination of phase contrast and

absorption. The reconstructed volumes contained isotropic voxels of 0.65 μm^3. Three specimens were tested to failure during SRCT scanning.

At the bundle scale, SRCT measurements were made on the ANATOMIX beamline [19]. Fibre bundles were glued vertically on sample holders for a standard goniometer head (Huber Diffraktionstechnik, Rimsting, Germany) and scanned above the glue. More details regarding the X-ray beam, the detector and objective used were given in a previous study [9].

2.5. 3D Microstructural analysis

Both bundle and composite volumes were analysed using the Avizo version 2021.1 software (Thermo Fisher Scientific, Waltham, Massachusetts, USA).

First, the reconstructed volume data files of flax/PLA composites were cropped to reduce their size; resulting in 1379 x 829 x 2048 voxel files. The materials were segmented by defining a threshold intensity value. First, all the pores were isolated from the rest of the internal composite matter: a thresholding segmentation tool was used to isolate the composite porosities, which included luminal cavities, pores of the cortical parenchyma residues and pores induced by the manufacturing process. All pores were represented by the darkest grey level. Then, each category of pores was manually isolated from the others using a very precise brush segmentation tool. Finally, they have been assigned a colour for the reader clarity. This analysis procedure was applied on six specimens including the three specimens tested to failure.

The procedure for fibre bundle analysis is identical to that used by Quereilhac et al [5]. The materials were segmented by defining a threshold intensity value. First, all pores of the internal fibre matter were isolated. Then, a precise brush segmentation tool was used to separate the lumen from the kink-bands porosity.

3. Results and discussion

3.1. Overall microstructure and main defects of flax fibre reinforced PLA UD composite

The reconstructed volumes of the three specimens tested to failure were carefully inspected. Figure 3 shows slices of the 3D reconstructed volume of the unload specimen 1, which includes all the

159 defects observed during the SRCT scans. Several features are visible, including (i) flax fibres assembled in
160 large bundles, (ii) flax fibre misalignment, (iii) presence of kink-bands, (iv) presence of cortical
161 parenchyma residues, and (v) pores, including luminal cavity, pores of the cortical parenchyma residues,
162 and pores induced by the manufacturing process.

163 Some features such as bundles, kink bands, cortical residues and luminal cavities are inherent
164 to plant fibres. By optimising the quality of the fibre extraction process (i.e. hackling), the level of fibre
165 individualisation can be improved [11] and the presence of cortical residues reduced [20]. However, like
166 other crop processing methods, mechanical extraction and especially breaking and beating (scutching)
167 induce numerous defects such as kink-bands [9,10]. A specific discussion below will address their
168 specific role in composite breakage.

169 Other defects, such as fibre misalignment, resin rich areas and the presence of large pores are
170 the result of the consolidation process. Among these defects, pores are one of the main factors
171 influencing their mechanical performance [21,22]. Figure 4 highlights the three types of pores contained
172 in the 6 analysed specimens. Large pores are located in resin-rich areas whereas pores of the cortical
173 residues are observed at the surface of fibre bundles, in which lumen cavities are visible. First, it was
174 noticed that porosity induced by the lumen and the cortical residue had similar values for the 6
175 specimens, respectively (0.35 ± 0.07) % and (0.06 ± 0.02) %. In contrast, discrepancies are observed
176 regarding the content of large pores with values ranging from 0.04 % to 1.86 %. The use of
177 thermoplastic resins such as PLA, which are more viscous than thermosets, and the film-stacking
178 processing route, both contribute to a high porosity content. Nevertheless, in the present case, porosity
179 induced by the process remains under 2% for the 6 samples, and between 0.36 and 2.36% in total,
180 which are acceptable values (table.1).

181

182 **3.2. The role of fibre misalignment and porosity on propagation of damage**

183 Having established that a number of microstructural features can be observed from the
184 tomograms, the following sections will focus on damage development during uniaxial loading. The three
185 specimens that were loaded during SRCT scanning showed an average failure strength of (174.3 ± 4.8)

MPa. Several studies reported slightly higher mechanical performances for equivalent fibre volume content [16,23–25] but mechanical characterisation protocol and specimen dimensions may account for differences. For example, time-dependent deformations of the material could occur during the SRCT experiment. The tensile tests to failure took around 15 mins versus around a minute with conventional tensile testing devices (linear strain without SRCT scanning).

For composite materials in tensile loading, damage events are mainly attributed to three damage modes: matrix shear cracks, interface splitting cracks attributed to fibre matrix debonding and fibre pull-out, and fibre breakage [15,26–28]. Their contribution and occurrence depends strongly on the composite microstructure and also on the nature and intrinsic specificities of its fibre and matrix phases.

A single test specimen (representative of all our observations) was chosen to describe the damage mechanisms (specimen A). Figure 5 shows a longitudinal section for a range of stress levels, demonstrating that in the present case, pores induced by the process and a misaligned bundle are the main defects. Crack initiates here from the edge of the notched specimen and propagates along the misaligned bundle interface. No shear cracks were observed around the large pores. It is interesting to note that no visible change in the microstructure was observed up to 88% of the stress at failure (Fig. 5c).

Figure 6 highlights a large misaligned bundle surrounded by large pores; notably, even this region remains undamaged until high levels of applied stress. Here cracks initiate from the curved bundle at 138 MPa, in contrast to above 150 MPa in the previous sequence (fig. 5). Rask et al found that damage evolution in unidirectional flax fibre yarn/polypropylene composites is initiated by interface splitting cracks from the notched area, followed by matrix shear cracks and ultimately fibre failures [15]. Similar observations on unidirectional flax fibre yarn/epoxy composites were made by Habibi et al [29]. They highlighted that the propagation of cracks along the unidirectional yarns is predominant in composite failure, leading to transverse matrix cracks and fibres breakage.

In composites, the fibre/matrix interface is considered as the primary region of stress transfer from the matrix to the fibre. Among thermoplastics, PLA has good adhesion properties on flax fibres, leading to good interface performance at the macro-scale [16]. However, both figures 5 and 6 indicate

214 that this interface is a zone of weakness, despite the good impregnation of the fibre reinforcement; in
215 plant fibre composites, the presence of residues such as cortical parenchyma, woody core or middle
216 lamellae components may play a major role in debonding or decohesion. Furthermore, after crop
217 processing, some cortical parenchyma residues could also remain on the fibre surfaces and by acting as
218 surface flaws, do not contribute in the stress transfer mechanisms between matrix and fibres [30].
219 Figure 7 highlights the propagation of cracks along fibres bundles in the area containing some cortical
220 residues. It is worth noting that debonding could occur either at the interface between the matrix and
221 the cortical residues or between the fibre surface and the cortical residues.
222 As mentioned in the introduction, flax fibres require special attention from extraction to
223 preform manufacturing. The quality of the field retting as well as the extraction process (breaking,
224 scutching and hackling) strongly affects the level of fibre individualisation and subsequent stress
225 distribution within the composite [11,31,32] . Guillou et al. explain that the preparation of well-aligned
226 fibre preforms requires additional hackling steps [20]. Although breaking and scutching process steps
227 have a major detrimental effect on the formation of dislocations (kink bands) on bast fibres [10,33,34].
228 Guillou et al. report that these additional drawing steps do not seem to affect the tensile properties of
229 elementary flax fibres [20]. In a recent work, Morgillo et al highlighted that flax fibres having undergone
230 breaking, scutching and hackling had more kink-bands, lower average kink-band area and surprisingly
231 better tensile properties than flax fibres having only undergone breaking process [35]. The previous
232 results demonstrate the interest to develop preforms with high levels of individualised fibres, highly
233 aligned fibres and low content of cortical residues. In the next section, a focus is proposed on the
234 involvement of kink-bands in composite damages.
235
236 **3.3. Highlighting the main role of kink-bands in composite breakage**
237 3.3.1. Focus on the specific structure of kink-bands
238 Even if the specific conditions in which these defects develop are not clearly understood yet,
239 their ultrastructure and shape has been widely investigated [4],[36]. These dislocations are often
240 referred to as zones of compression creases or slip-lines to illustrate the deviation of cellulose micro-

241 fibrils. Figure 8 shows a 3D visualisation of a scutched flax fibre bundle containing major dislocations
242 across the whole section and Figure 9 shows details of kink-bands on more individualized flax fibres.
243 These micro-CT observations on isolated bundles and fibres help understand the complex distribution of
244 pores induced by local cell-wall deformations.

245 Fig.8.B shows a typical "X" shape with a longitudinal symmetrical organisation of pores across
246 the whole bundle section. It is worth to note that kink-band formation could either occur at the same
247 location when fibres are still packed in bundles or occur at various position along individualised fibres
248 (Fig. 9). In both examples, kink-bands are the result of stress loading occurring due to bending or
249 buckling during the fibres' scutching stages.

250 Fig. 9.C shows the porous ultrastructure of kink-bands observed from SRCT measurement at the
251 bundle scale on the ANATOMIX beamline. The 3D renderings clearly exhibit the concentric dislocation
252 areas of the S2-G cell-wall layer of flax fibres, organised around the lumen. Their porous ultrastructure
253 was also studied by Quereilhac et al. [5]. However, no quantification of kink-band porosities was
254 performed on SRCT measurements conducted at the composite scale at the PSICHE beamline, due to
255 limitation in spatial resolution.

256

257 3.3.2. The strong link between composite breakage and kink-bands

258 Careful inspection of the 3D reconstructed volumes revealed that individual fibres and fibre
259 bundles failed at the highest stress level (above 150 MPa). The 2D slices of specimen 1, in figures 10, 11
260 and 12, show that fibre failure occurs exactly at the kink-band area, but no major evolution of the kink-
261 band microstructure is visible until failure. However, in Figure 11, crack openings can be seen in the
262 matrix surrounding the kink-band area. Eichhorn et al [37] found that such defects in flax and hemp
263 fibres act as stress concentration areas in the matrix, potentially leading to crack initiation and
264 fibre/matrix debonding. This stress concentration was quantified by Hughes et al. using half-fringe
265 photoelasticity [38]. In close surrounding area of the kink-band, stress concentrations of up to 1.4 were
266 reported, inducing matrix micro cracks.

Fig.12 shows crack initiation in a kink-band area, leading to transverse failure from the outer surface towards the centre of the fibre. Similar results were reported by Madsen et al [28]. Regarding fibre bundle failures, a more complex mechanism was put forward by Aslan [39] and confirmed by Beaugrand et al [40]. It is reported that fibre bundle failure could involve longitudinal and transverse failures between adjacent kink-bands, also referred to as crack-bridging. However, in the present study, it appears that fibres fail in a more brittle manner resulting in a single transverse fracture surface, as observed in Figures 10, 11 and 12.

The failure mechanism at macroscale can be explained by Cook and Gordon model [41] . This work clarifies the phenomena of crack propagation in a composite, the role of the fibres being particularly significant, as the cracks created in the matrix can propagate into the fibre or along the interface, leading to interface debonding. This mechanism arises from the existence of relatively small stresses working in the same direction as the crack, situated slightly ahead of the propagating cracks. In the case of a sufficiently weak matrix/fibre interface, these stresses lead to an opening of the interface ahead of the crack, which serves to blunt the crack and thereby reduce stress concentration at the crack tip, making it energetically favourable for the crack to propagate along the interface [28]. Interestingly, Figure 13 confirms the propagation of crack through the fibres, as proposed by Cook and Gordon's.

In the present study, the observations of the fracture pathways highlighted in Figure 13 support the hypothesis that fibre failure is the most critical damage mechanism. Cracks propagate along the large fibre bundles (yellow lines in figure.13) and transverse fibre failure occur at the exact position of kink-bands.

3.3.3. Critical length *versus* inter kink-band distance

Previous observation of ultimate fibre failure at the kink-band sites raises the question of the ability of the fibre to transfer stress through the composite. In this last section, we compare the critical fibre length to the average kink-band distance. The critical fibre length can be defined as the fibre length required for the interfacial shear stress to load the fibre to its fracture stress. Below the critical fibre

length, fibres pull-out at composite rupture. Fibre length inferior to the critical fibre length L_c is defined by Eq.(1) [42], where σ_f is the fibre tensile strength (at the critical fibre length), d_f is the fibre diameter, and τ is the interfacial strength. As inputs in Eq.1, fibre tensile strength (1090 MPa) and flax-PLA interfacial shear stress (15.6 MPa) have been used from a study of Pantaloni et al. [16].

$$L_c = \frac{\sigma_f \times d_f}{2\tau} \qquad \text{(Eq. 1)}$$

The critical fibre lengths are calculated for fibre element diameters from 4 to 400 µm, considering both elementary fibres and fibre bundles (Fig. 14).

Figure 14 shows the evolution of the calculated critical length for fibre element diameters from 4 to 400 µm (black points). The blue points were calculated from the experimental tensile values of each Flaxtape single fibre. The average kink-bands inter distance has been evaluated through analysis of 3D volumes and SEM, on 20 and 100 single flax fibres, respectively. The average distance measured from micro-CT and SEM images is (76±23) µm and (82±31) µm, respectively. The two values are in the same range. The dotted horizontal line in Figure 16 represents the averaged kink-band inter distance of (79±27) µm.

In all cases, whatever the fibre or bundle diameter, the kink-band inter distance is always lower than the critical fibre length; this result confirms the main role of kink-bands in damage development in plant fibre composites. Indeed, in most of the cases, kink-bands drive and induce fibre breakage without any debonding. This fundamental link between the fibre critical length and the kink-band density confirms the important need in preserving fibres during extraction process, by limiting the number of defects and also in optimizing the retting stages so that to favour smoother extraction processes.

4. Conclusions

This experimental investigation highlights the main features of flax fibres involved in damage evolution of an unidirectional flax / PLA composite loaded in uniaxial tension. Analysis of *in-situ* SRCT tomographs shows that the composite microstructure exhibits specific features: some are inherent to

plant fibres such as bundles, kink bands, cortical residues and luminal cavities; others, such as resin rich areas, presence of large pores and fibre misalignment are defects related to the consolidation process. Even if the presence of fibre misalignment and large pores is not detrimental regarding crack initiation in the case of PLA based composite, these features still play a significant role in the propagation of damages. Similarly, the presence of parenchyma cortical residues along the fibre surfaces was found to promote interface splitting cracks, leading to an inhomogeneous distribution of stress between fibres. This confirms the interest to develop preform with a high level of individualised fibres, highly aligned fibres and low cortical residue content. Such reinforcement quality can be achieved by additional hackling and stretching steps. Although processing steps tend to lead to a larger number of kink-bands, the resulting fibres do not show lower tensile properties. However, at the composite scale, the presence of kink-bands is critical regarding fibre failure. This work clearly evidences that fibre transverse failure occurs at the exact position of kink-bands, whether for elementary fibres or for fibre bundles.

Future investigations need to be carried out on additional batches of flax fibre reinforcement (i.e scutched, hackled, stretched) to understand the impact of kink-band morphology, such as porosity and surface area, on the fibre failure mechanisms within composites. Also, flax tow could be considered as a potential reinforcement, as long as the kink-band inter distance remains inferior to the critical fibre length.

Credit for authorship contribution statement

Elouan Guillou: Investigation, Conceptualization, Writing-original draft, Writing-review & editing. **Andrew King:** Methodology, Software, Writing-review & editing. **Jonathan Perrin:** Methodology, Software. **Henry Proudhon:** Methodology, Software, Writing-review & editing. **Timm Weitkamp:** Methodology, Software, Writing-review & editing. **Darshil U. Shah:** Conceptualization, Writing-review & editing. **Alexandre Beigbeder:** Investigation, Supervision. **Pierre Ouagne:** Investigation, Conceptualization, Writing-review & editing, Supervision. **Alain Bourmaud:** Investigation, Conceptualization, Writing-review & editing, Supervision.

Declaration of competing interest

The authors declare that they have no known competing financial interests or personal relationships that could have appeared to influence the work reported in this paper.

Acknowledgements

The authors would like to gratefully acknowledge Laval Agglomération (https://www.agglo-laval.fr) and the Région Pays de Loire (https://www.paysdelaloire.fr/) for PhD funding. ANATOMIX is an Equipment of Excellence (EQUIPEX) funded by the Investments for the Future Programme of the French National Research Agency (ANR), project NanoimagesX, grant no. ANR-11-EQPX-0031. Access to the Anatomix and Psiche beamlines was provided through SOLEIL beamtime proposals #20201291 and #20220533.

References

[1] Baley C, Bourmaud A, Davies P. Eighty years of composites reinforced by flax fibres: A historical review. Compos Part A Appl Sci Manuf 2021;144:106333. https://doi.org/10.1016/j.compositesa.2021.106333.

[2] Shah DU, Schubel PJ, Clifford MJ. Can flax replace E-glass in structural composites? A small wind turbine blade case study. Compos Part B Eng 2013;52:172–81. https://doi.org/10.1016/j.compositesb.2013.04.027.

[3] Bensadoun F. In-service behaviour of flax fibre reinforced composites for high performance applications 2016.

[4] Melelli A, Durand S, Arnould O, Richely E, Guessasma S, Jamme F, et al. Extensive investigation of the ultrastructure of kink-bands in flax fibres. Ind Crops Prod 2021;164. https://doi.org/10.1016/j.indcrop.2021.113368.

[5] Quereilhac D, Pinsard L, Guillou E, Fazzini M, De Luycker E, Bourmaud A, et al. Exploiting synchrotron X-ray tomography for a novel insight into flax-fibre defects ultrastructure. Ind Crops

Prod 2023;198:116655. https://doi.org/10.1016/j.indcrop.2023.116655.

[6] Baley C. Influence of kink bands on the tensile strength of flax fibers 2004;9:331–4.

[7] Grégoire M, Barthod-Malat B, Labonne L, Evon P, De Luycker E, Ouagne P. Investigation of the potential of hemp fibre straws harvested using a combine machine for the production of technical load-bearing textiles. Ind Crops Prod 2020;145:111988. https://doi.org/10.1016/j.indcrop.2019.111988.

[8] Hughes M. Defects in natural fibres: Their origin, characteristics and implications for natural fibre-reinforced composites. J Mater Sci 2012;47:599–609. https://doi.org/10.1007/s10853-011-6025-3.

[9] Bourmaud A, Pinsard L, Guillou E, De Luycker E, Fazzini M, Perrin J, et al. Elucidating the formation of structural defects in flax fibres through synchrotron X-ray phase-contrast microtomography. Ind Crops Prod 2022;184:115048. https://doi.org/10.1016/j.indcrop.2022.115048.

[10] Kozlova L, Petrova A, Chernyad'ev A, Salnikov V, Gorshkova T. On the origin of bast fiber dislocations in flax. Ind Crops Prod 2022;176:114382. https://doi.org/10.1016/j.indcrop.2021.114382.

[11] Coroller G, Lefeuvre A, Le A, Bourmaud A, Ausias G, Gaudry T, et al. Composites : Part A Effect of flax fibres individualisation on tensile failure of flax / epoxy unidirectional composite. Compos Part A 2013;51:62–70. https://doi.org/10.1016/j.compositesa.2013.03.018.

[12] Summerscales J, Dissanayake N, Virk A, Hall W. A review of bast fibres and their composites. Part 2 - Composites. Compos Part A Appl Sci Manuf 2010;41:1336–44. https://doi.org/10.1016/j.compositesa.2010.05.020.

[13] Richely E, Bourmaud A, Dhakal H, Zhang Z, Beaugrand J, Guessasma S. Exploring the morphology of flax fibres by X-ray microtomography and the related mechanical response by numerical modelling. Compos Part A Appl Sci Manuf 2022;160:107052. https://doi.org/10.1016/j.compositesa.2022.107052.

[14] Drouhet Q, Touchard F, Chocinski-Arnault L, Mellier D. 3D strain fields in a plant fibre composite during fragmentation test: Micro-CT based DIC and DVC. Compos Part B Eng 2023;263:110860.

https://doi.org/10.1016/j.compositesb.2023.110860.

[15] Rask M, Madsen B, Sørensen BF, Fife JL, Martyniuk K, Lauridsen EM. Composites : Part A In situ observations of microscale damage evolution in unidirectional natural fibre composites. Compos Part A 2012;43:1639–49. https://doi.org/10.1016/j.compositesa.2012.02.007.

[16] Pantaloni D, Rudolph AL, Shah DU, Baley C, Bourmaud A. Interfacial and mechanical characterisation of biodegradable polymer-flax fibre composites. Compos Sci Technol 2021;201:108529. https://doi.org/10.1016/j.compscitech.2020.108529.

[17] Ghorpade VM, Gennadios A, Hanna MA. Laboratory composting of extruded poly(lactic acid) sheets. Bioresour Technol 2001;76:57–61. https://doi.org/10.1016/S0960-8524(00)00077-8.

[18] Pantaloni D, Shah D, Baley C, Bourmaud A. Monitoring of mechanical performances of flax non-woven biocomposites during a home compost degradation. Polym Degrad Stab 2020;177:109166. https://doi.org/10.1016/j.polymdegradstab.2020.109166.

[19] Weitkamp T, Scheel M, Perrin J, Daniel G, King A, Le Roux V, et al. Microtomography on the ANATOMIX beamline at Synchrotron SOLEIL. J Phys Conf Ser 2022;2380. https://doi.org/10.1088/1742-6596/2380/1/012122.

[20] Guillou E, Bar M, Scheel M, Falher T, Weitkamp T, Shah DU, et al. Use of a commingling process for innovative flax fibre reinforced unidirectional composites. Compos Part B 2024;270:111150. https://doi.org/10.1016/j.compositesb.2023.111150.

[21] Madsen B, Lilholt H. Physical and mechanical properties of unidirectional plant fibre composites — an evaluation of the influence of porosity 2003;63:1265–72. https://doi.org/10.1016/S0266-3538(03)00097-6.

[22] Richely E, Beaugrand J, Coret M, Binetruy C, Ouagne P, Bourmaud A, et al. In Situ Tensile Testing under High-Speed Optical Recording to Determine Hierarchical Damage Kinetics in Polymer Layers of Flax Fibre Elements. Polymers (Basel) 2023;15:2794. https://doi.org/10.3390/polym15132794.

[23] Sanivada UK, Mármol G, Brito FP, Fangueiro R. PLA Composites Reinforced with Flax and Jute. Polymers (Basel) 2020;12:1–29.

[24] Khanlou HM, Woodfield P, Summerscales J, Francucci G, King B, Talebian S, et al. Estimation of

mechanical property degradation of poly(lactic acid) and flax fibre reinforced poly(lactic acid) bio-composites during thermal processing. Meas J Int Meas Confed 2018;116:367–72. https://doi.org/10.1016/j.measurement.2017.11.031.

[25] Lebrun G, Couture A, Laperrière L. Tensile and impregnation behavior of unidirectional hemp/paper/epoxy and flax/paper/epoxy composites. Compos Struct 2013;103:151–60. https://doi.org/10.1016/j.compstruct.2013.04.028.

[26] Dogossy G, Czigány T. Failure mode characterization in maize hull filled polyethylene composites by acoustic emission. Polym Test 2006;25:353–7. https://doi.org/10.1016/j.polymertesting.2005.12.004.

[27] Marec A, Thomas JH, El Guerjouma R. Damage characterization of polymer-based composite materials: Multivariable analysis and wavelet transform for clustering acoustic emission data. Mech Syst Signal Process 2008;22:1441–64. https://doi.org/10.1016/j.ymssp.2007.11.029.

[28] Madsen B, Aslan M, Lilholt H. Fractographic observations of the microstructural characteristics of flax fibre composites. Compos Sci Technol 2016;123:151–62. https://doi.org/10.1016/j.compscitech.2015.12.003.

[29] Habibi M, Laperrière L, Lebrun G, Toubal L. Combining short flax fiber mats and unidirectional flax yarns for composite applications: Effect of short flax fibers on biaxial mechanical properties and damage behaviour. Compos Part B Eng 2017;123:165–78. https://doi.org/10.1016/j.compositesb.2017.05.023.

[30] Le Duigou A, Kervoelen A, Le Grand A, Nardin M, Baley C. Interfacial properties of flax fibre-epoxy resin systems: Existence of a complex interphase. Compos Sci Technol 2014;100:152–7. https://doi.org/10.1016/j.compscitech.2014.06.009.

[31] Baley C, Gomina M, Breard J, Bourmaud A, Drapier S, Ferreira M, et al. Specific features of flax fibres used to manufacture composite materials. Int J Mater Form 2019;12. https://doi.org/10.1007/s12289-018-1455-y.

[32] Tanguy M, Bourmaud A, Beaugrand J, Gaudry T, Baley C. Polypropylene reinforcement with flax or jute fibre; Influence of microstructure and constituents properties on the performance of composite. Compos Part B Eng 2018;139:64–74.

https://doi.org/10.1016/j.compositesb.2017.11.061.

[33] Hernandez-Estrada A, Gusovius HJ, Müssig J, Hughes M. Assessing the susceptibility of hemp fibre to the formation of dislocations during processing. Ind Crops Prod 2016;85:382–8. https://doi.org/10.1016/j.indcrop.2016.01.006.

[34] Hänninen T, Thygesen A, Mehmood S, Madsen B, Hughes M. Mechanical processing of bast fibres: The occurrence of damage and its effect on fibre structure. Ind Crops Prod 2012;39:7–11. https://doi.org/10.1016/j.indcrop.2012.01.025.

[35] Morgillo L, Brionne L, Melelli A, Ouagne P, Scheel M, Weitkamp T, et al. Elucidating links between the mechanical performance of flax fibres and their structural defects. Ind Crops Prod 2023;206. https://doi.org/10.1016/j.indcrop.2023.117722.

[36] Nyholm K, Ander P, Bardage S, Daniel G. Dislocations in pulp fibres - Their origin, characteristics and importance - A review. Nord Pulp Pap Res J 2001;16:376–84. https://doi.org/10.3183/npprj-2001-16-04-p376-384.

[37] Eichhorn SJ, Baillie CA, Zafeiropoulos N, Mwaikambo LY, Ansell MP, Dufresne A, et al. Current international research into cellulosic fibres and composites. J Mater Sci 2001;36:2107–31. https://doi.org/10.1023/A:1017512029696.

[38] Hughes M, Sébe G, Hague J, Hill C, Spear M, Mott L. An investigation into the effects of micro-compressive defects on interphase behaviour in hemp-epoxy composites using half-fringe photoelasticity. Compos Interfaces 2000;7:13–29. https://doi.org/10.1163/156855400300183551.

[39] Aslan M, Chinga-Carrasco G, Sørensen BF, Madsen B. Strength variability of single flax fibres. J Mater Sci 2011;46:6344–54. https://doi.org/10.1007/s10853-011-5581-x.

[40] Beaugrand J, Guessasma S, Maigret JE. Damage mechanisms in defected natural fibers. Sci Rep 2017;7:1–7. https://doi.org/10.1038/s41598-017-14514-6.

[41] Cook J, Gordon JE, Evans CC, Marsh DM. A mechanism for the control of crack propagation in all-brittle systems. Proc R Soc London Ser A Math Phys Sci 1964;282:508–20. https://doi.org/10.1098/rspa.1964.0248.

[42] Kelly A, Tyson WR. Tensile properties of fibre-reinforced metals: Copper/tungsten and

483 copper/molybdenum. J Mech Phys Solids 1965;13. https://doi.org/10.1016/0022-
484 5096(65)90035-9.
485

Figures caption

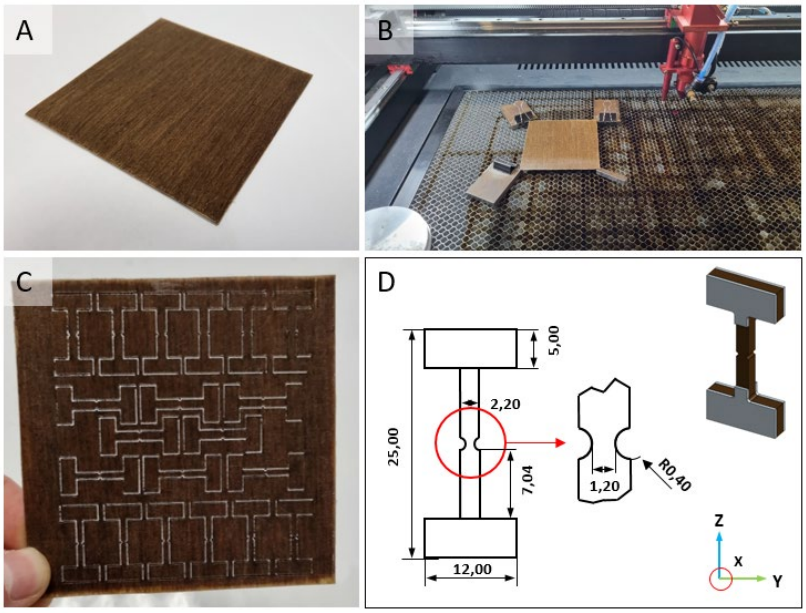

Figure 1. PLA-flax UD composite (A); Laser cutting set-up (B); Tensile specimens after cutting (C) and Drawings and dimensions (in mm) with 3D representation of the specimen (D).

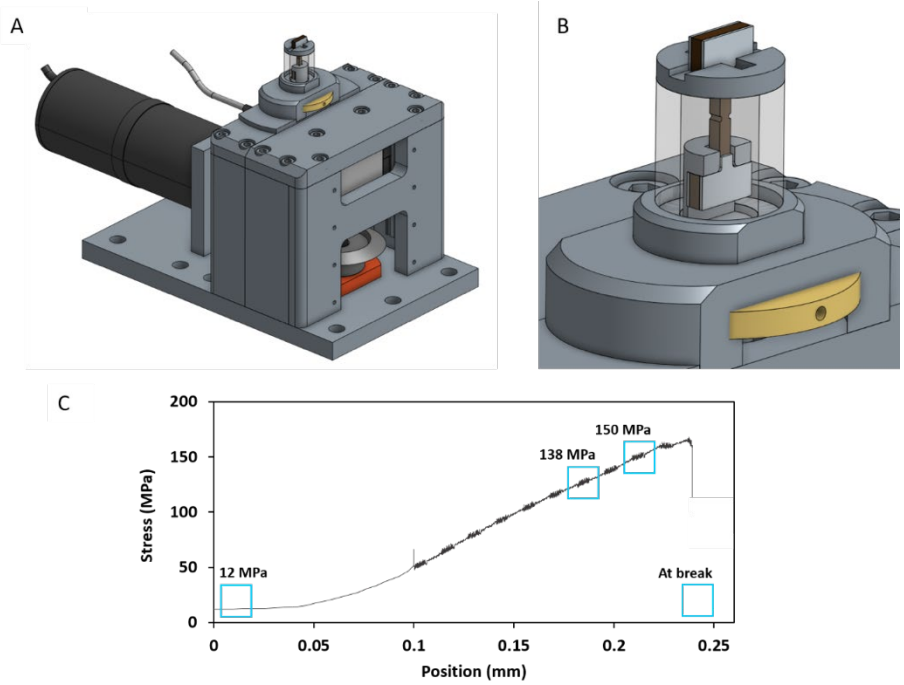

Figure 2. (A) Sketch of the tensile stress rig Bulky; (B) Close-up view of the Flax Fibre Composite specimen mounted in Bulky, visible through the PMMA tube; (C) Specimen 1 loading curve until failure: The blue boxes indicate the selected scan positions that will be described in section 3.

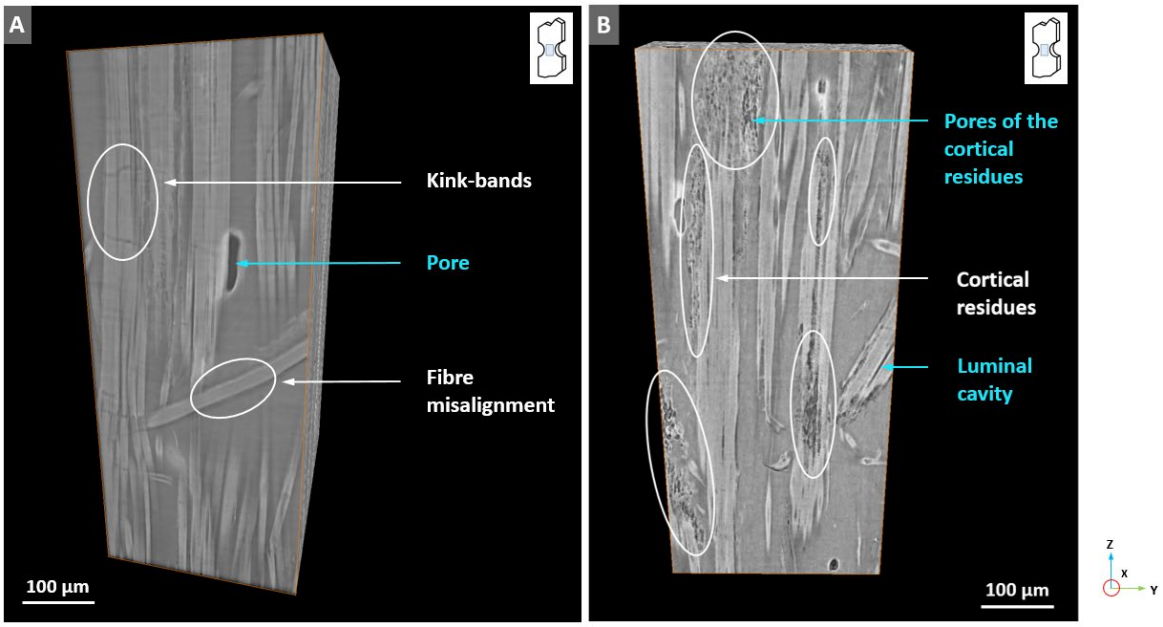

Figure 3. PLA-flax fibre UD volume from post-failure micro-CT acquisition, highlighting examples of typical defects such as fibre kink-bands, pores, or fibre misalignment (A), luminal cavity, cortical residues and their containing pores (B).

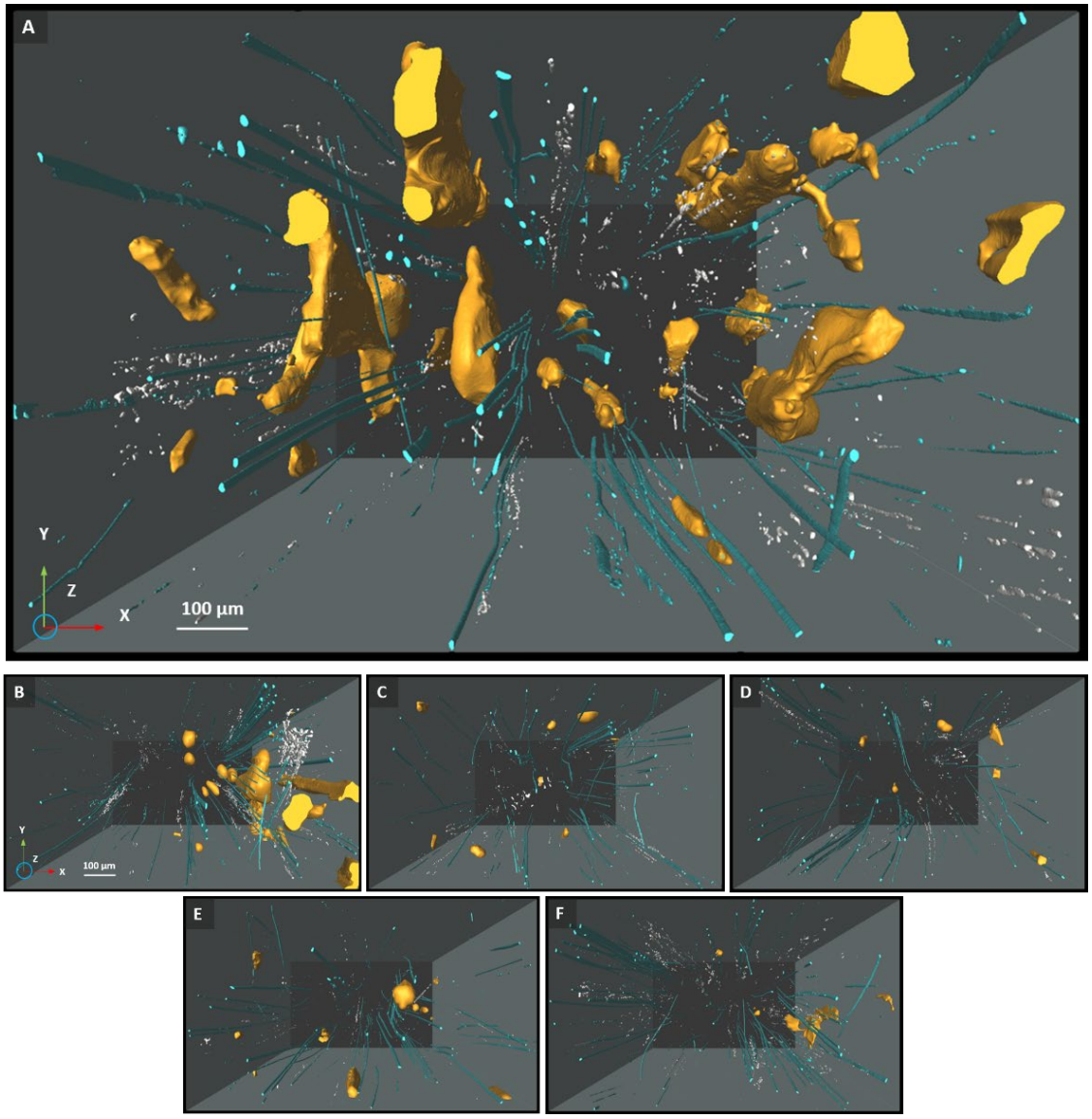

Figure 4. 3D visualisation of lumen cavities in blue, process pores in yellow and pores contained in the cortical parenchyma residues in white according to samples A to F. For each sample, the analysed volume is 0.641 mm^3.

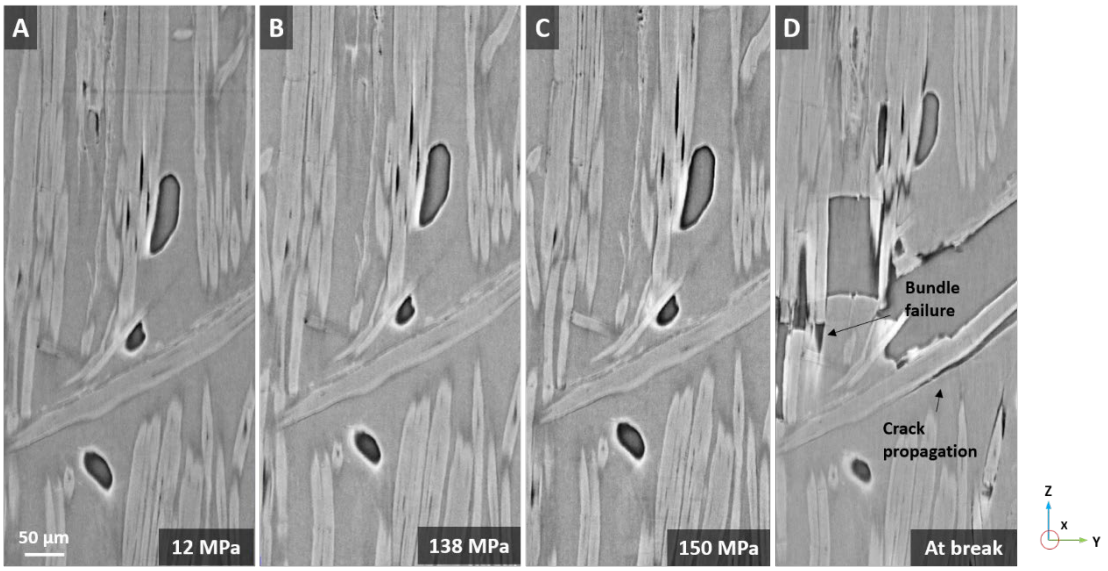

Figure 5. Propagation of crack along misaligned bundle. Images from tomographic scans of specimen 1 at different stress level.

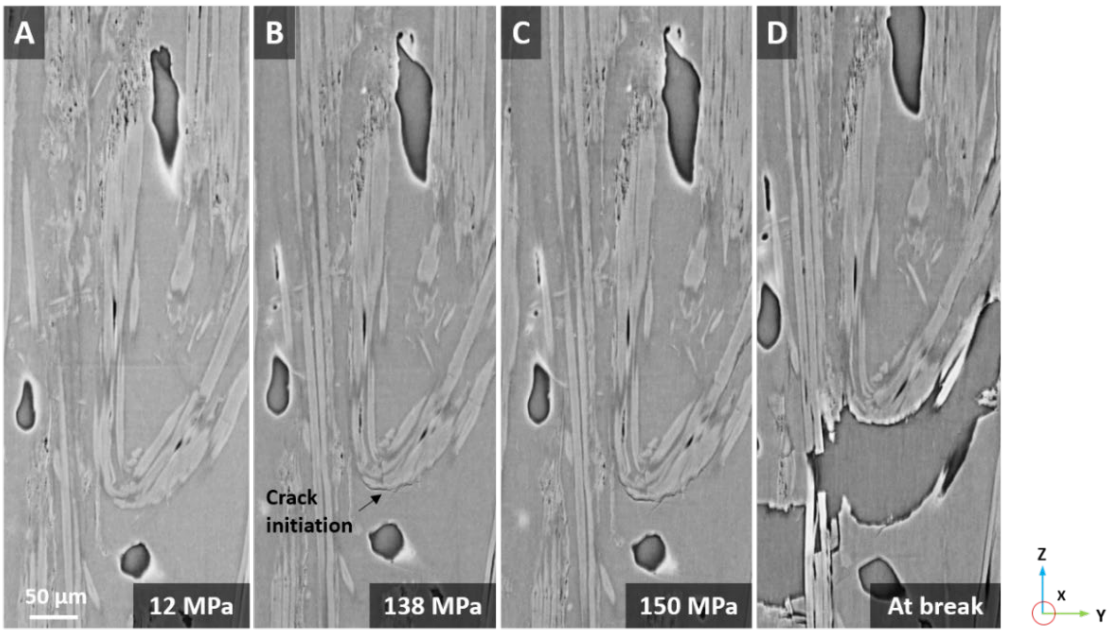

Figure 6. Initiation of crack at a curve bundle. Images from tomographic scans of the specimen 1 at different stress.

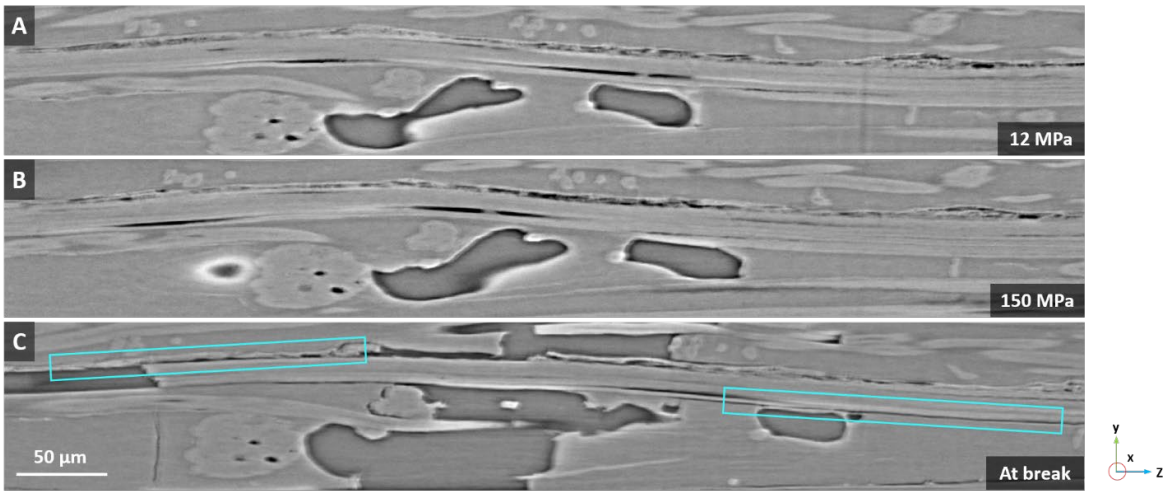

511

512 **Figure 7**. Cracks propagation along fibre bundles at interfaces areas. Images from tomographic scans of

513 specimen 1 at different stress levels

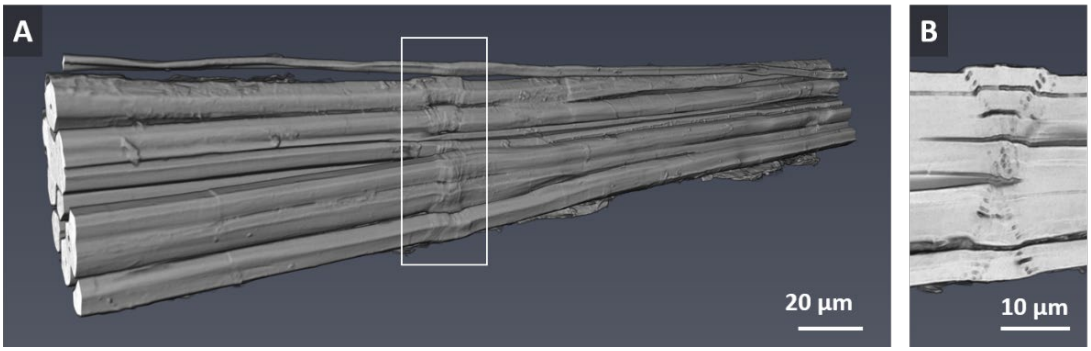

514

515 **Figure 8**. Flax bundle 3D rendering (A) with a specific zoom on a cross-longitudinal view of the kink band

516 area (B).

517

518

519

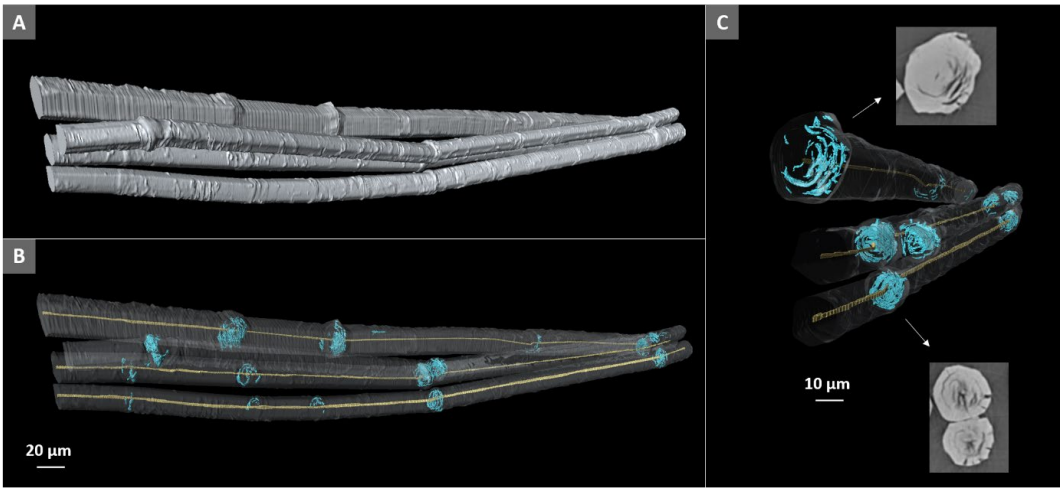

Figure 9. 3D renderings of hackled flax fibres with surface of the fibres (A), voids within the fibres including lumen in yellow and kink band induced porosities in blue (B), 3D visualisation of kink-band porosities around the lumen with the corresponding tomographic slices of the fibre cross sectional area (C).

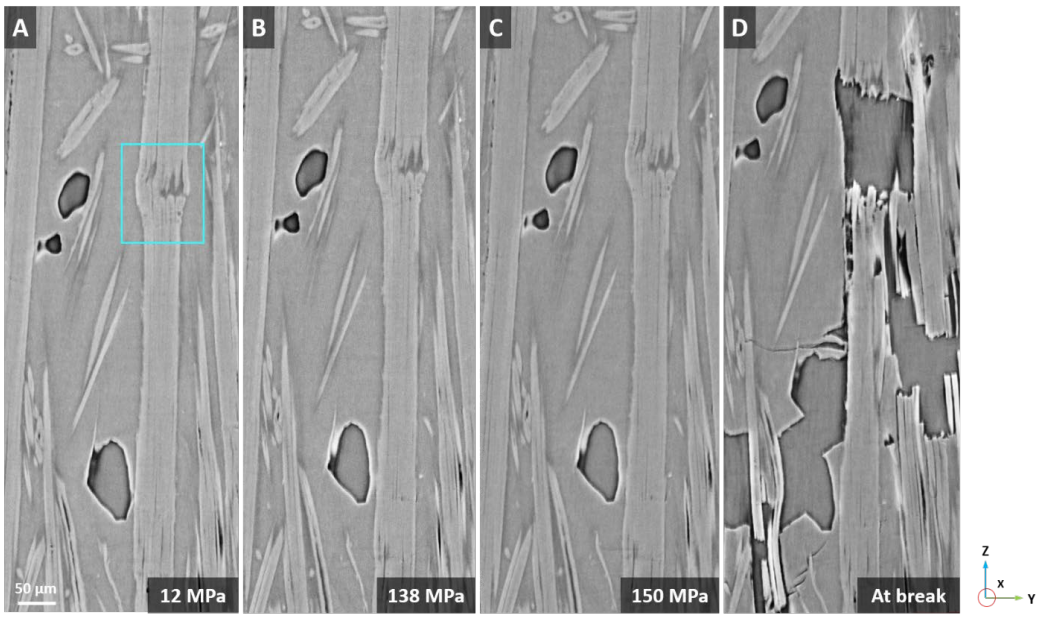

Figure 10. Images from tomographic scans of the specimen 1 at different stress levels until failure with focus on kink-bands impact on damage development: the area of kink-band before tensile loading (A) is highlighted through a blue square.

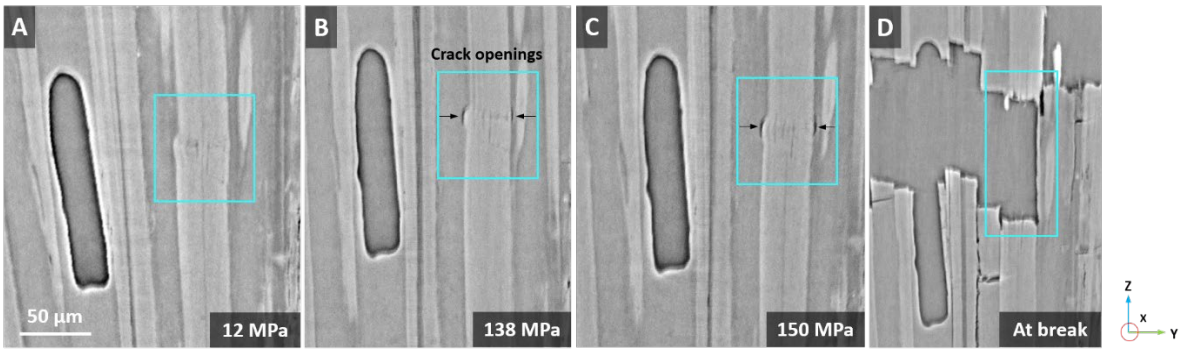

Figure 11. Images from tomographic scans of the specimen 1 at different stress level with focus on kink-band impact on damage development.

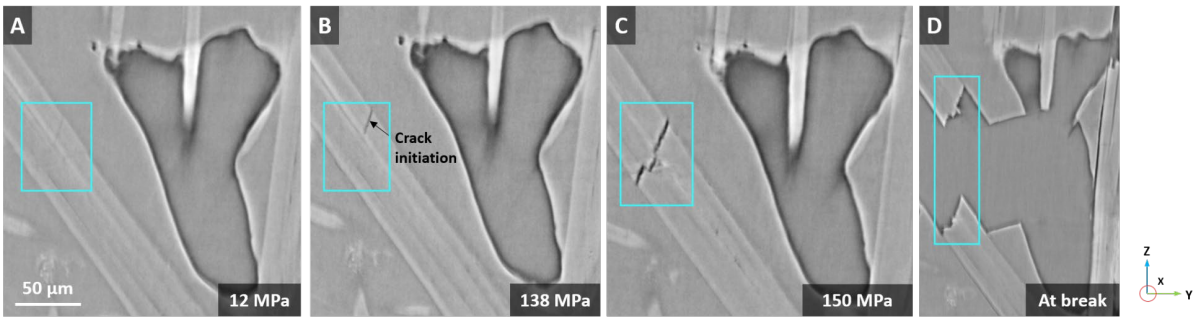

Figure 12. Images from tomographic scans of the specimen 1 at different stress level with focus on kink-band breakage during loading.

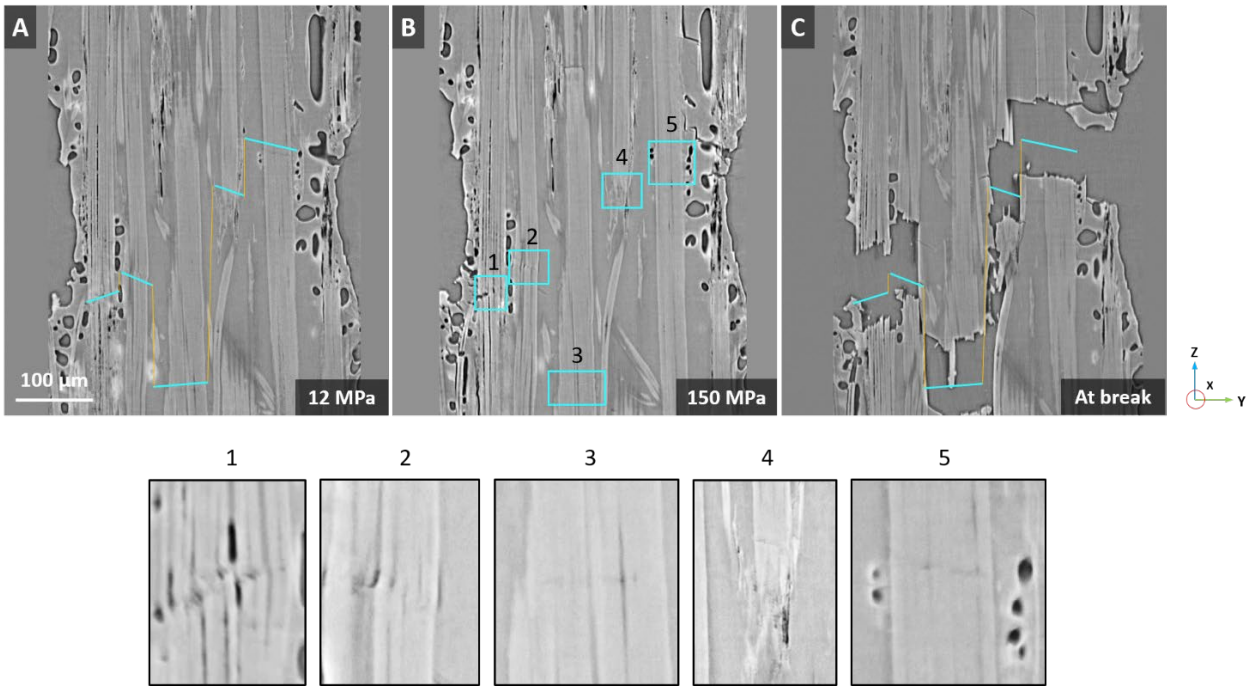

539

540 **Figure 13**. Fracture pathways of specimen 1 at different stress levels (A,B and C) with a specific zoom on

541 kink-ban areas (1,2,3,4 and 5). The yellow lines highlight longitudinal cracks propagation along fibre

542 bundles.

543

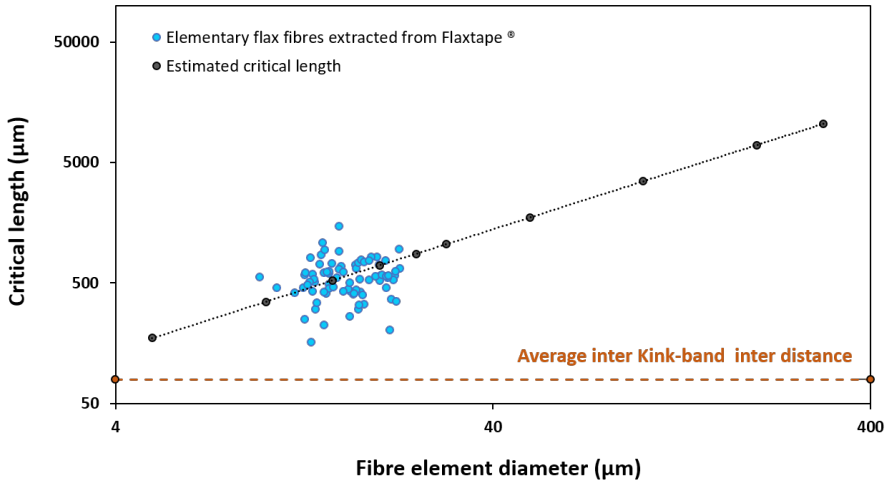

544

545 **Figure 14**. Evolution of the critical length for flax element diameter from 4 to 400 µm.

546

547

548 **Table 1.** Porosity of the 6 analysed composite samples induced by fibres (f), process (p) and cortical

549 residues (CR)

Sample ID	A	B	C	D	E	F
Porosity f (%)	0.43	0.40	0.27	0.31	0.27	0.39
Porosity p (%)	1.86	1.01	0.06	0.04	0.26	0.14
Porosity CR (%)	0.07	0.08	0.03	0.06	0.02	0.07
Total (%)	2.36	1.49	0.36	0.41	0.55	0.6

550